Supplementary Information (SI) for Journal of Materials Chemistry A.

Supporting information: Pt single atoms/g-C_3N_4 photocatalysts enabling simultaneous H_2 production and CO_2 absorption through formic acid photoreforming

Xu Liu, Zhehao Sun, Yi-Lun Chen, Kaili Liu, Muhammad Usman, Lucy Gloag, Zongyou Yin**

† X.L. and Z.S. contributed equally to this work.

* E-mail: lucy.gloag@anu.edu.au & zongyou.yin@anu.edu.au

Research School of Chemistry, Australian National University, ACT 2601, Australia.

GC calibration

H_2 is calibrated by using a 100 μL injector measuring 50 μL and 100 μL H_2 (4%), using a 250 μL injector measuring 150 μL, 200 μL and 250 μL H_2 (4%), and integrating peak area between 3.0 min to 4.0 min, the result is shown in the table below. Degassing a 22.5 mL vial with Ar, inject 225 μL H_2, then mix gas with stirring. Taking 100 μL mixed gas will be equivalent to taking 1 μL H_2 (4%). The calibration data and linear fitting curve of H_2 are shown in **Table S1** and **Fig. S1**.

Table S1. The H_2 volume and corresponding area for calibration.

No.	Gas	Gas Volume (μL)	H_2 Volume (μL)	Area
1	Ar	0	0	0
2	$_{Ar,}$ 4% H_2	1	0.04	11
3	4% H_2	50	2	2070
4	4% H_2	100	4	4220
5	4% H_2	150	6	6345
6	4% H_2	200	8	8457
7	4% H_2	250	10	10581

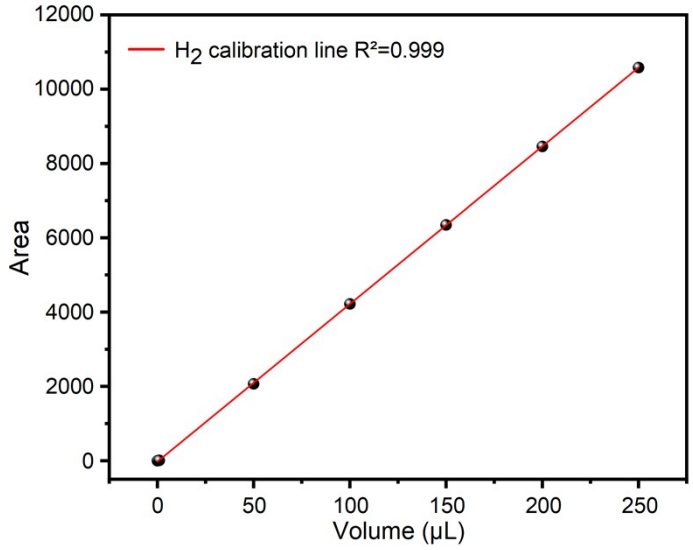

Fig. S1. The fitting curve of H_2 calibration in GC.

TCD line resolves H_2 (3.2 min), O_2 (~5.5 min), and N_2 (~7.4 min), and the H_2 yield can be calculated by the following formulas.

$$Rate = \frac{(Area + 64) \times P_{H_2} \times V_{gas} \times \eta}{22.4 \times 42.6 \times V_{measure} \times t \times m} \ (\mu mol \cdot g^{-1} \cdot h^{-1})$$

$$\eta = \frac{V_{measure}}{V_{measure} - \left(v_{H_2} + v_{CO_2}\right)}$$

where *Area* is the peak area read directly from GC; P_{H2} is the percentage of H_2 in standard gas in this case is 3.91%; V_{gas} is the total gas volume in reaction vial; *22.4 (L/mol)* is the molar volume of ideal gas under standard conditions; $V_{measure}$ is the gas volume in injector; *t* is reaction time; *m* is the mass of catalyst. The unit of V_{gas} and $V_{measure}$ should united. Since the production of various gases creates additional pressure in the reactor, η is a correction factor used here to correct for yield errors, and v_{H2}, v_{CO2}, v_{CO} and so on are the volumes of the various gases in the injector, which are calculated from each individual calibration curve.

CO_2 is calibrated by using a 100 μL injector measure 50 μL and 100 μL CO_2, using a 250 μL injector measure 150 μL, 200 μL and 250 μL CO_2, and integrating peak area between 4.0 min to 5.0 min; the result is shown in the table below. Degassing a 22.5 mL vial with Ar, inject 225 μL CO_2, then mix gas with stirring. Taking 100 μL mixed gas will be equivalent to taking 1 μL CO_2. The calibration data and linear fitting curve of H_2 are shown in **Table S2** and **Fig. S2**.

Table S2. The CO_2 volume and corresponding area for calibration

No.	Gas	CO_2 Volume (μL)	CO_2 mole (μmol)	Area
1	Ar	0	0	0
2	Ar, CO_2	1	0.045	103325
3	CO_2	50	2.23	6269047
4	CO_2	100	4.46	10826463
5	CO_2	150	6.7	16890000
6	CO_2	200	8.93	23511023
7	CO_2	250	11.16	28591518

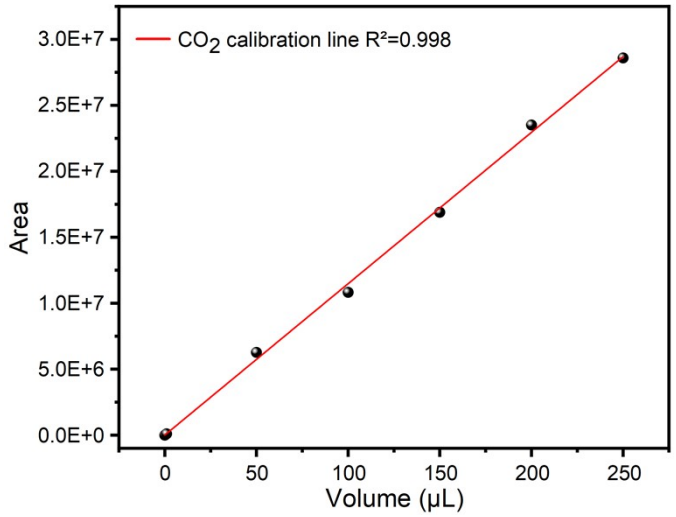

Fig. S2. The fitting curve of CO_2 calibration in GC.

FID line resolves CO_2 (4.5 min) and the CO_2 emission can be calculated by following the formula,

$$Rate = \frac{(Area + 1465) \times V_{gas} \times \eta}{22.4 \times 1.418 \times 10^5 \times V_{measure} \times t \times m} \ (\mu mol \cdot g^{-1} \cdot h^{-1})$$

where parameters are same as defined above.

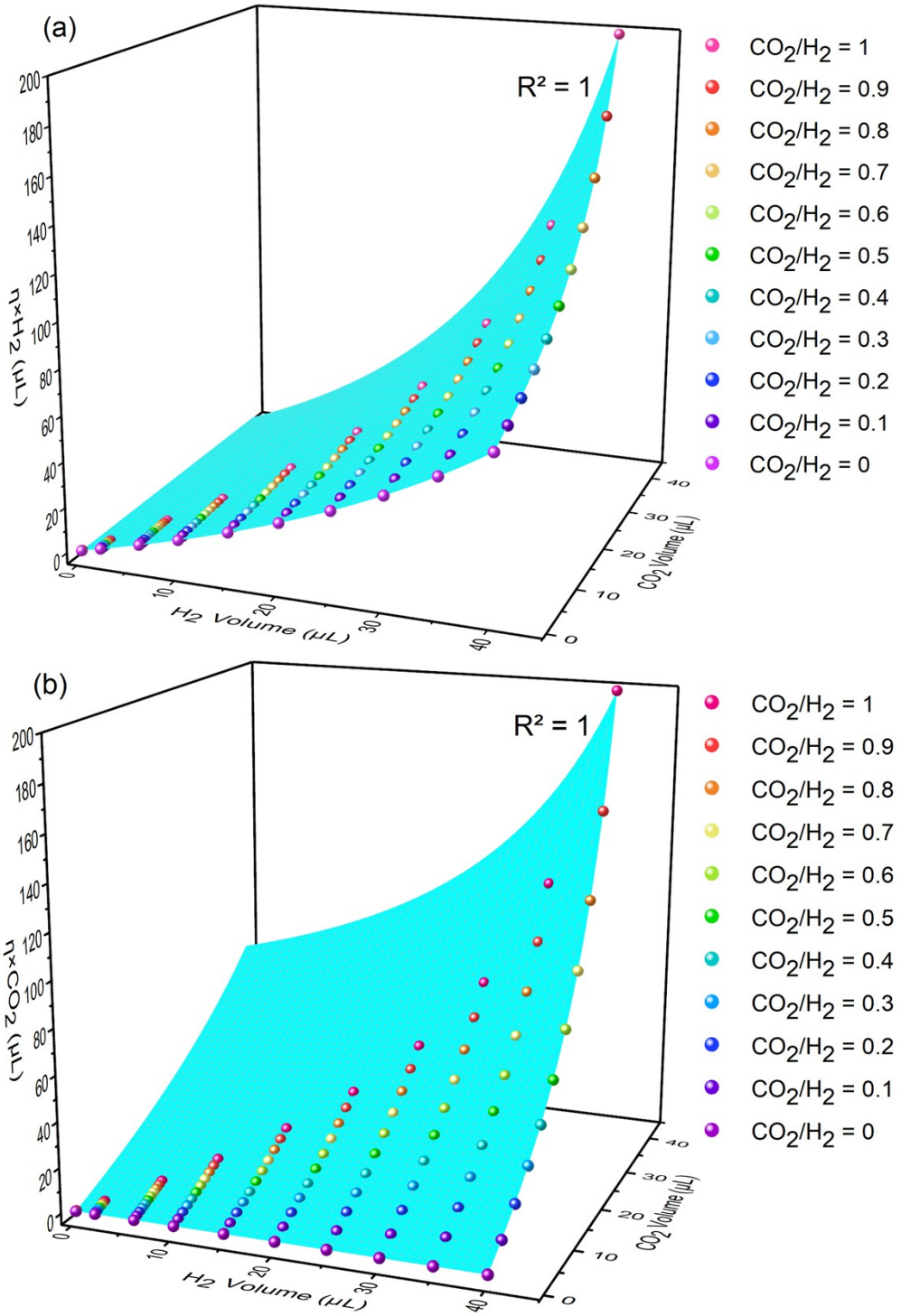

Fig. S3. 3D fitted surface representing **(a)** the H_2 volume and **(b)** the CO_2 volume corrected by the η in $V_{measure}$ = 100 μL systems with different ratios of H_2 and CO_2.

Table S3. ICP-AES-determined Pt content of Pt on g-C_3N_4 catalysts with varying nominal loadings.

Sample (Nominal Pt wt%)	Measured Pt loading by ICP-AES (wt%)
0.125 wt% Pt on g-C_3N_4	0.12
0.25 wt% Pt on g-C_3N_4	0.22
0.5 wt% Pt on g-C_3N_4	0.43
1.1 wt% Pt on g-C_3N_4	1.03
2.0 wt% Pt on g-C_3N_4	1.84
5.0 wt% Pt on g-C_3N_4	5.05

Table S4. Gas production rates for single-atom Pt on g-C_3N_4 during formate dehydrogenation, as determined by gas chromatography (GC) catalysts in 4 M FA at pH 2.2. NA denotes values below the GC detection limit. The unit is μmol/g/h.

	CO_2	CO	CH_4	H_2	N_2	O_2
g-C_3N_4	NA	13	NA	619	NA	NA
0.125 wt% Pt on g-C_3N_4	361	45	NA	19194	NA	NA
0.25 wt% Pt on g-C_3N_4	702	61	NA	27102	NA	NA
0.5 wt% Pt on g-C_3N_4	1707	63	NA	42093	NA	NA
1.1 wt% Pt on g-C_3N_4	2003	80	NA	55787	NA	NA

Table S5. Comparison of photocatalytic activity of 1.1 wt% Pt on g-C_3N_4 with other photocatalysts for the dehydrogenation of FA.

	Material	Medium	Light source	Stability	H_2 (or CO) Yield	Selectivity	Reference
This work	1.1 wt% Pt on g-C_3N_4	4M FA aqueous solution (pH 2.2)	300 W Xenon lamp (Microsolar 300, PerfectLight) with a 420 nm cut-off filter (AM 1.5)	> 48 h	**55.8 mmol·g^{-1}h^{-1}**	100%	this work
	0.5 wt% Pt on g-C_3N_4	4M FA aqueous solution (pH 2.2)	300 W Xenon lamp (Microsolar 300, PerfectLight) with a 420 nm cut-off filter (AM 1.5)	/	42.1 mmol·g^{-1}h^{-1}	100%	this work
	0.25 wt% Pt on g-C_3N_4	4M FA aqueous solution (pH 2.2)	300 W Xenon lamp (Microsolar 300, PerfectLight) with a 420 nm cut-off filter (AM 1.5)	/	27.1 mmol·g^{-1}h^{-1}	100%	this work
	0.125 wt% Pt on g-C_3N_4	4M FA aqueous solution (pH 2.2)	300 W Xenon lamp (Microsolar 300, PerfectLight) with a 420 nm cut-off filter (AM 1.5)	/	19.1 mmol·g^{-1}h^{-1}	100%	this work
	1.1 wt% Pt on g-C_3N_4	4M FA aqueous solution (pH 12.2)	300 W Xenon lamp (Microsolar 300, PerfectLight) with a 420 nm cut-off filter (AM 1.5)	/	5 mmol·g^{-1}h^{-1}	100%	this work
Pt-based catalysts	0.025 wt% Pt-CdS	5.0 mL formic acid in 100 mL distilled water	400W Hg lamp	> 12h	1.22 mmol·g^{-1}h^{-1}	/	1
	Co-CN-Pt	10 vol % formic acid with H_2PtCl_6 solution (Pt 8 wt %)	300W xenon lamp with an output power of 5.9 W. (300–1100 nm)	> 30 h	9.039 mmol·g^{-1}h^{-1}	99.98%	2
	Pt/PCN	98.68 mL formic acid solution (0.70 mol L^{-1}), and 1.32 mL of H_2PtCl_6 (1.93×10^{-3} mol L^{-1})	300 W Xenon lamp with intensity of 103 mW cm^{-2} in full-spectrum	> 20 h	1.6 mmol·g^{-1}h^{-1}	/	3

	PCN/TiO_2/Pt	formic acid solution (2.7 M, 10 vol%)	300 W Xenon lamp (300 mW/cm^2)	> 25 h	11.1 mmol·$g^{-1}h^{-1}$	/	4
	Au@SiO_2-Pt	10 mL DI water containing 100μL of formic acid solution (98%)	300 W Xenon lamp with a 420-nm cutoff filter	> 3 h	/	/	5
Other catalysts	UiO-66$(COOH)_2$-Cu	0.24% FA (2400 ppm)	150 W Xe lamp (Hamamatsu LC8, irradiance = 71 mW/cm^2) with a >390 nm high-pass filter	> 3 d	5 mmol·$g^{-1}h^{-1}$	100%	6
	Co–Ni/CdS NRs	FA (2 mL) with sodium formate (3.0 M)	Xenon lamp (750 W, 45 A) 100 mW cm^{-2} λ>420 nm, 25 °C	> 18 h	32.6 mmol·$g^{-1}h^{-1}$	100%	7
	CdS/2D $V_{0.1}W_{0.9}N_{1.5}$	1 M FA aqueous solution	Xenon lamp (Microsolar 300, Beijing Perfectlight, AM 1.5G filter), with an intensity of approximately 0.56 W/cm^2	> 12 h	46.01 mmol·$g^{-1}h^{-1}$	87.1%	8
	AuPd/TiO_2 nanofibers	2.7 M FA aqueous solution	Solar simulator (67005, Newport Corp.) standard AM 1.5 sunlight (100 mW cm^{-2})	> 9 h	17.7 mmol·$g^{-1}h^{-1}$	98%	9
	PdAg(NWs)@ g-C_3N_4	1M FA aqueous solution	Visible Light (λ > 400 nm)	> 3 h	11.5 mmol·$g^{-1}h^{-1}$	/	10
	AgPd/CN	5 M NaCOOH +88% FA (v:v = 19.5:1)	300 W Xenon lamp (Newport Corporation)	> 4.5 h	71.1 mmol·$g^{-1}h^{-1}$	/	11
	AuPd/CNS	100 ml 1.0 M of HCOOH and HCOONa (mole ratio = 4:1)	300 W Xenon lamp	> 1.25 h	201 mmol·$g^{-1}h^{-1}$	/	12
	Au@Pd/UiO-66(Zr85Ti15)	4% Formic acid solution	500 W Xenon lamp (> 420 nm, 320 mW cm^{-2})	> 3 h	11.2 mmol·$g^{-1}h^{-1}$	/	13

$Cu/Cu_2O/CuO/TiO_2$	2.7 M FA aqueous solution	standard AM 1.5 sunlight (100 mW cm^{-2})	> 12 h	2.54 $mmol·g^{-1}h^{-1}$	/	14
$Ni_2P/Zn_3In_2S_6$	6.6 M FA aqueous solution	The 300W Xe light (PLS-SXE300, Beijing Trusttech Co. Ltd, China)	> 12 h	6.4 $mmol·g^{-1}h^{-1}$	/	15
$MoP/Zn_3In_2S_6$	6.0 M FA solution (without plus sacrificial reagent	300 W Xe lamp equipped with a 400 nm cutoff filter (λ > 400 nm)	> 10 h	0.927 $mmol·g^{-1}h^{-1}$	/	16
Co-sal-NH_2-MIL-68@In_2S_3	10 μL FA + 1.8 mL DMA+0.2 mL H_2O, and 45 mg BIH	300 W Xe lamp (PLS-SXE300+＞420 nm)	> 24 h	18.746 $mmol·g^{-1}h^{-1}$	99.9%	17
R-B TiO_2 MSCs	20 mL 6.6 M FA solution	Xe lamp (300 W, λ > 325 nm) with intensity of 11 $mW·cm^{-2}$	> 500 h	30.4 $mmol·g^{-1}h^{-1}$	99%	18
CdS NRs/Fe–salen complexes	4M Formic acid in H_2O and CH_3CN (v:v=1:1)	300 W Xe lamp equipped with UV cut-off filter (λ > 420 nm)	> 30 h	H_2: 150 $mmol·g^{-1}h^{-1}$ CO: 71.5 $mmol·g^{-1}h^{-1}$	67.7%	19
CdS/W_2N_3	mixture of FA and DI water	300 W Xe lamp (λ > 420 nm)	> 54 h	H_2: 131 $mmol·g^{-1}h^{-1}$ CO: 103.5 $mmol·g^{-1}h^{-1}$	55.9%	20
$In_2S_3/Cd_{0.9}Zn_{0.1}S$	6 M formic acid in H_2O with NaOH	300 W xenon lamp	> 36 h	H_2: 100 $mmol·g^{-1}h^{-1}$ CO: 102 $mmol·g^{-1}h^{-1}$	49.5%	21
FeP@CdS nanorod	4 M formic acid, pH 3.5	300 W Xe lamp equipped with a UV cutoff filter (λ > 420 nm)	>4 d	H_2: 278 $mmol·g^{-1}h^{-1}$	100%	22
CoP@RGO/CdS	6.6M formic acid aqueous solution	White LED (30 × 3 W, λ≥ 420 nm) 11 $mW·cm^{-2}$	> 168 h	H_2: 182 $mmol·g^{-1}h^{-1}$	99.5%	23

CdS/CNTs NRs/Fe porphyrin	4 M formic acid with 0.04 mM catalyst (Fe-porphyrin) in 20 mL acetonitrile and water (1:3) mixture	300 W Xe lamp UV cutoff filter (λ > 420 nm)	> 20 h	H_2: 205.5 mmol·$g^{-1}h^{-1}$ CO: 126 mmol·$g^{-1}h^{-1}$	62%	24
NiCoP@CdS NRs	4 M FA aqueous solution at pH 3.5	300 W Xe lamp UV cut-off filter (λ > 420 nm)	> 48 h	H_2: 354 mmol·$g^{-1}h^{-1}$	100%	25

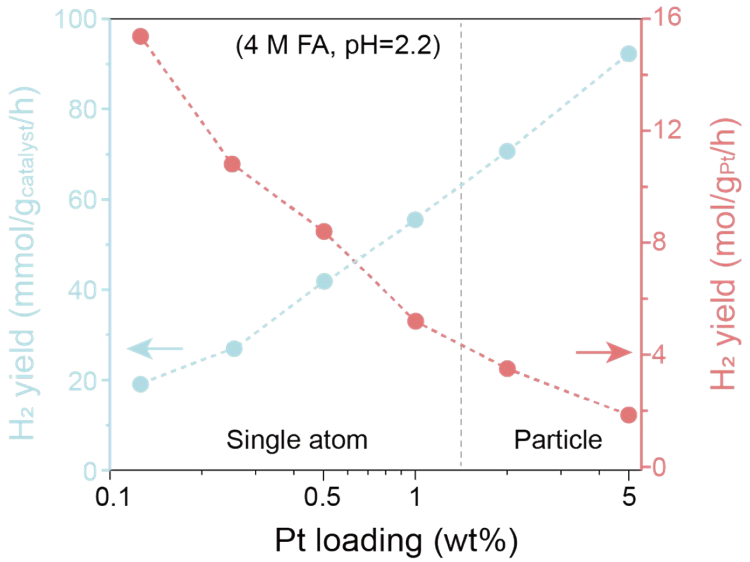

Fig. S4. Photocatalytic H_2 yield (left axis) and Pt mass activity (right axis) as a function of Pt loading for Pt/g-C_3N_4 catalysts under FA photoreforming conditions (4 M FA, pH = 2.2).

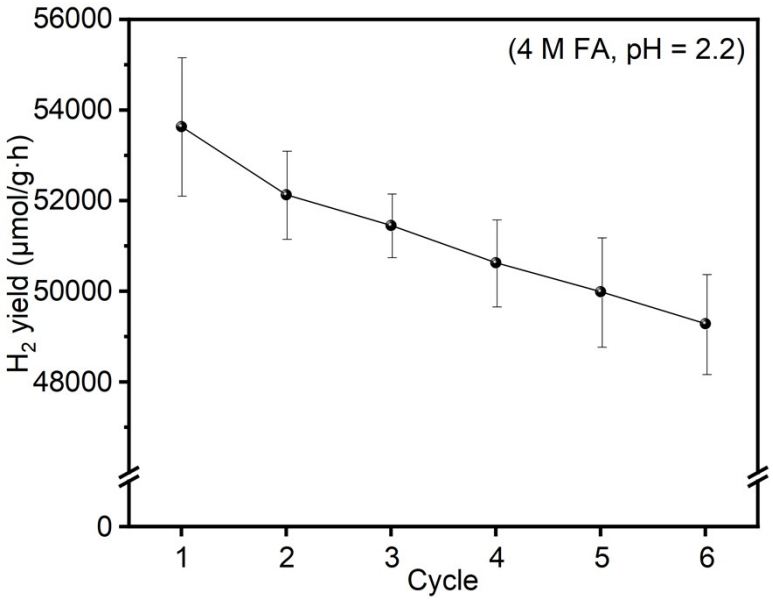

Fig. S5. The average photocatalytic performance during each cycle, along with the standard deviation in 4 M FA at pH 2.2.

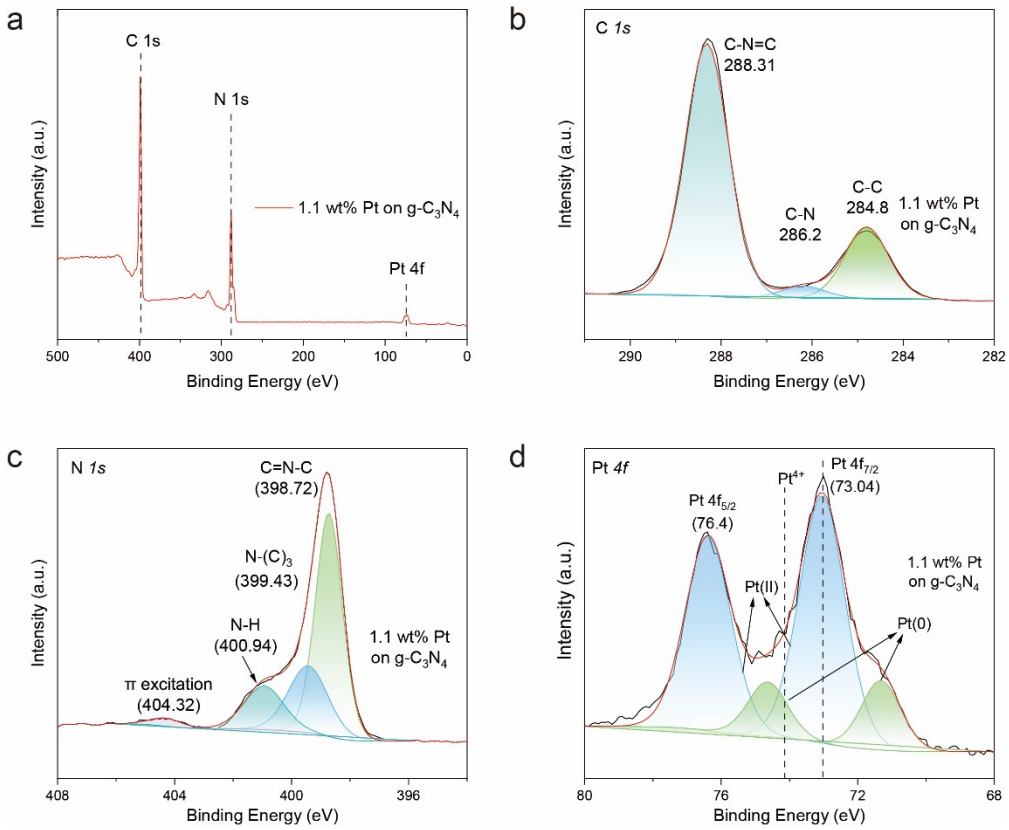

Fig. S6. XPS spectra of the 1.1 wt% Pt on g-C_3N_4 catalyst after photocatalytic stability testing. (a) Survey spectrum showing the characteristic C 1s, N 1s, and Pt 4f signals. (b) C 1s (c) N 1s (d) Pt 4f with no significant shift compared to the fresh sample, confirming the preserved chemical environment and stability of Pt single atoms.

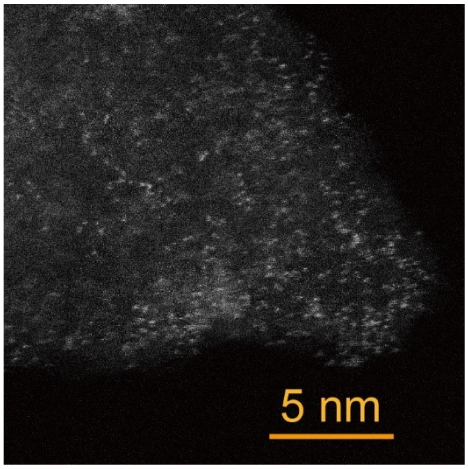

Fig. S7. High resolution HAADF-STEM image of 1.1 wt% Pt on g-C_3N_4 after 48 h of photocatalytic formic acid dehydrogenation. Isolated bright spots corresponding to Pt single atoms remain well-dispersed, with no observable nanoparticle formation, confirming structural stability.

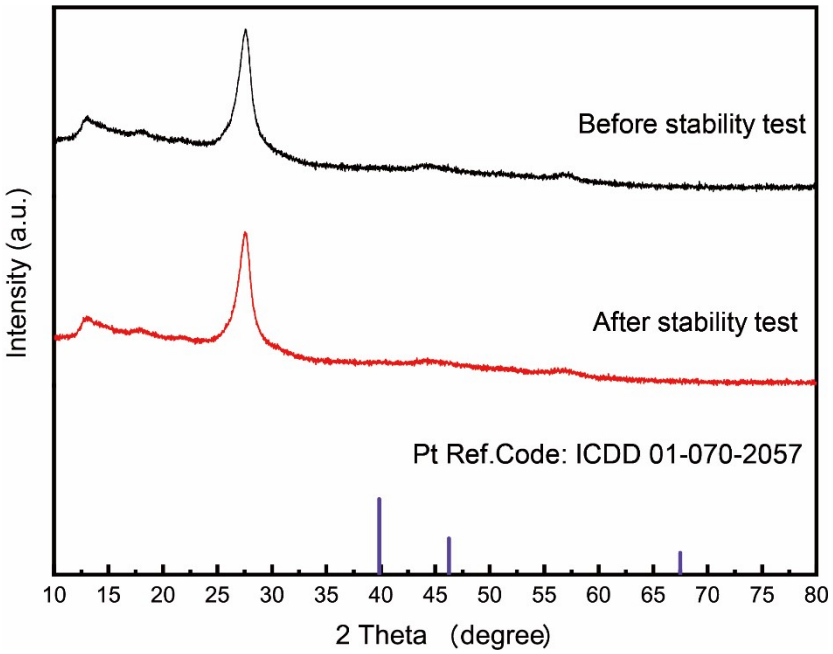

Fig. S8. XRD patterns of 1.1 wt% Pt on g-C_3N_4 catalysts before and after stability test.

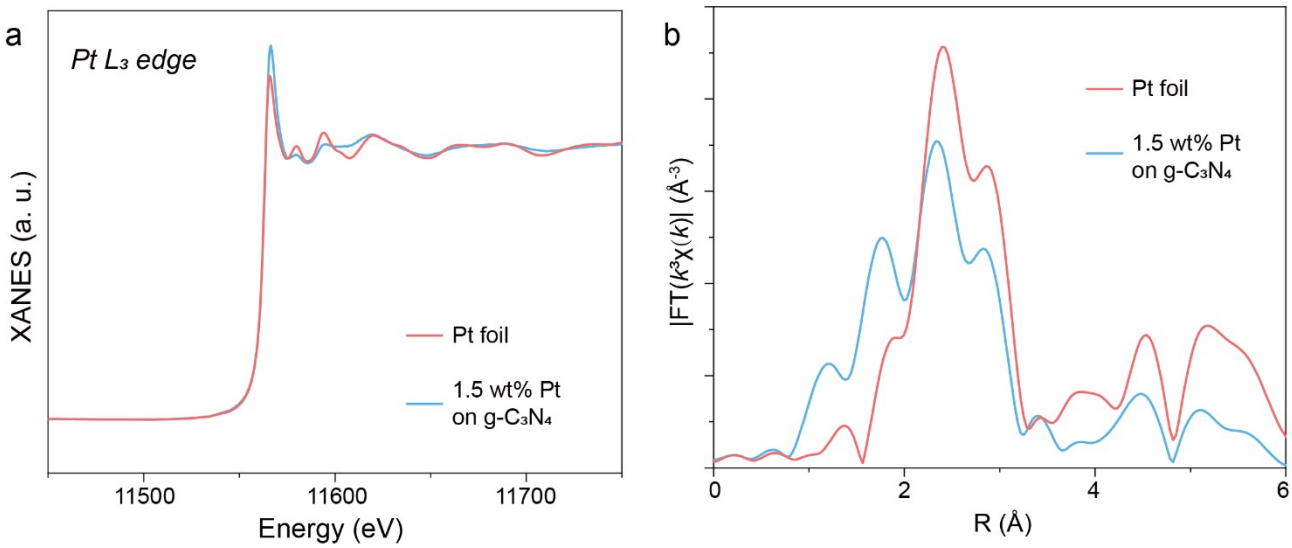

Fig. S9. (a) Normalized XANES spectra near the Pt L_3-edge and (b) Fourier transformation of the EXAFS spectra for 1.5 wt% Pt on g-C_3N_4 and reference samples.

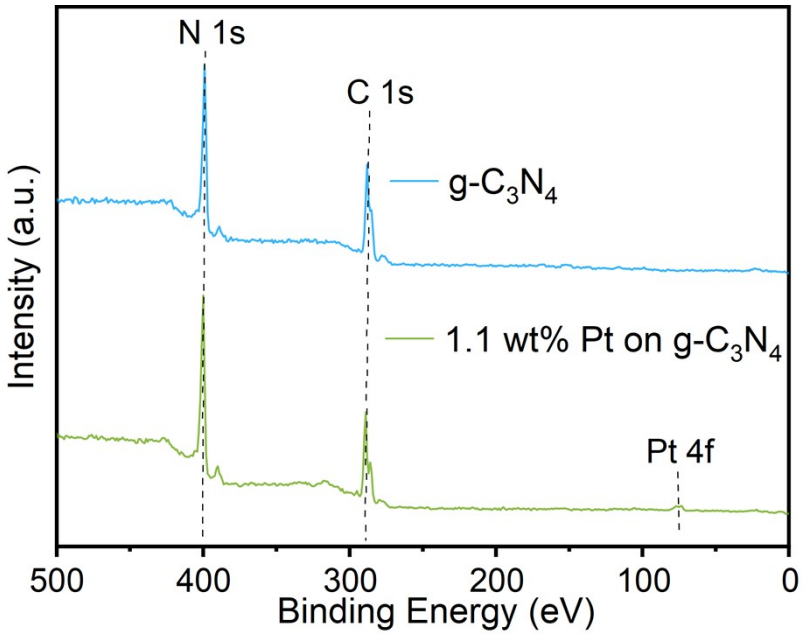

Fig. S10. XPS full survey spectra.

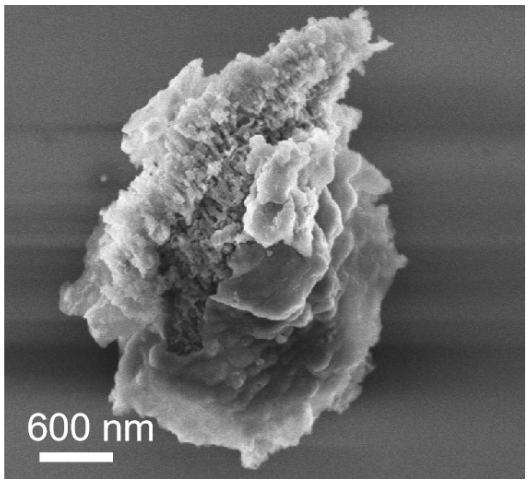

Fig. S11. SEM characterization of the 1.1 wt% Pt on g-C_3N_4 at 50× magnification.

Table S6. Elemental composition in 1.1 wt% Pt on g-C_3N_4 by EDX.

Element	Line Type	wt%
C	K series	57.39
N	K series	41.54
Pt	M series	1.07
Total:		100

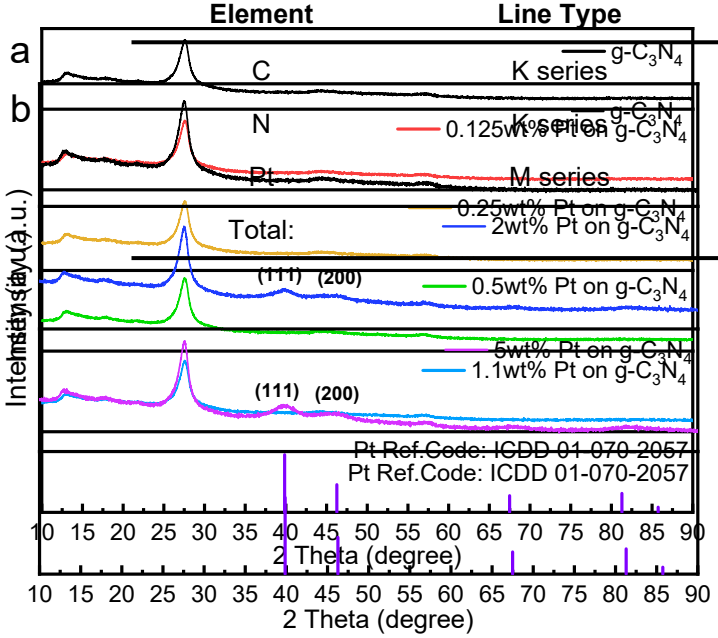

Fig. S12. XRD patterns of **(a)** g-C_3N_4 and g-C_3N_4 with different Pt single atom loading, **(b)** g-C_3N_4 with larger amount of Pt loading.

Fig. S12 shows that the original g-C_3N_4 displays a weak XRD diffraction peak at 2θ = 13.2° and a wider peak at 2θ =27.6°, assigned to the characteristic (100) and (002) planes, which represent the in-plane packing of heptazine units and interlayer stacking

of g-C_3N_4 sheets, respectively.[26] Pt SA on g-C_3N_4 samples still guarantee the structural characteristic peaks of g-C_3N_4, and no corresponding Pt diffraction peaks appear, indicating that the basic structure of g-C_3N_4 remained stable after anchoring Pt and indirectly proving that there are no metal particles. When the loading amount of Pt was continuously added up to 2 wt% and even 5 wt%, the XRD patterns showed the (111) and (200) crystal planes of Pt, indicating the formation of Pt nanoparticles.

Table S7. Comparison of Pt loading of 1.1 wt% Pt on g-C_3N_4 with other carbon-supported SACs.

	Material	Pt loading (wt%)	Pt size or density	Reference
Pt SACs on carbon-based supports	1.1 wt% PtSA on g-C_3N_4	1.1	4 Pt atoms per nm^2	This work
	Pt on Mesoporous zeolite	0.5	/	[27]
	Pt on N-doped C	0.4	0.01 Pt atoms per nm^2	[28]
	Pt on phosphomolybdic acid-modified active carbon	0.91	/	[29]
	Pt on covalent triazine frameworks	2.8	/	[30]
	Pt on g-C_3N_4	0.35	size of 0.1 nm - 0.2 nm	[31]
	Pt on N-doped porous carbon	0.73	0.034 Pt atom per nm^2	[32]
	Pt on nitrogen-doped nanocarbon	0.8	/	[33]
	Pt_1/Fe_2O_3	0.9	<0.5 Pt atoms per nm^2	[34]
	Pt/Al_2O_3	0.28	100% dispersion	[35]
	Pt_1/FeO_x	0.17	0.07 Pt atoms per nm^2	[36]
	Pt/TiN	0.35	/	[37]
	Pt/MoS_2	0.2	100% isolated Pt monomers	[38]
	Pt/MoS_2	7.5	65.5% neighbouring Pt monomers and 23.7% patches of Pt	[38]
	Pt@CdS	0.98	/	[39]
	Pt1-$Pr_4Ni_3O_{10+\delta}$	3	/	[40]
	$Pt/FAPbBr_{3-x}I_x$	1.8	/	[41]
	Pt_{SA}-NiO/Ni	1.14	/	[42]
Pt SACs on metal-based supports	$Pt/Ce_{0.9}Zr_{0.1}O_2$-X	1.1	/	[43]

Pt/Pd SAA	1.1	/	44
Pt1/CuO-CeO_2	0.83	/	45
$Mo_2TiC_2T_x$–Pt_{SA}	1.2	/	46
$Ti_3C_2T_x$-Pt_{SA}	0.84	/	47
Pt/CeO_2	3.06	0.99 Pt atoms per nm^2	48
Pt/TiO_2	2.1	0.7 Pt atoms per nm^2	49
Pt/CeO_2-polyhedra	1	1.1 Pt atoms per nm^2	50
Pt1/SiO_2–N	0.3	0.31 Pt atoms per nm^2	51
Pt on polyhedral ceria	1	1.1 Pt atoms per nm^2	52
Pt(0.25)/TiO_2	0.25	0.14 Pt atoms per nm^2	53
Pt-CdS	3	0.67 Pt atoms per nm^2	54
0.8Pt/CeO_2	0.37	0.8 Pt atoms per nm^2	55
Pt-decorated TiO_2 nanosheet	0.78	0.14 Pt atoms per nm^2	56
Pt1/Fe_2O_3	1.66	1.2 Pt atoms per nm^2	57
Pt/K/$MgAl_2O_4$	1	0.3 Pt atoms per nm^2	58

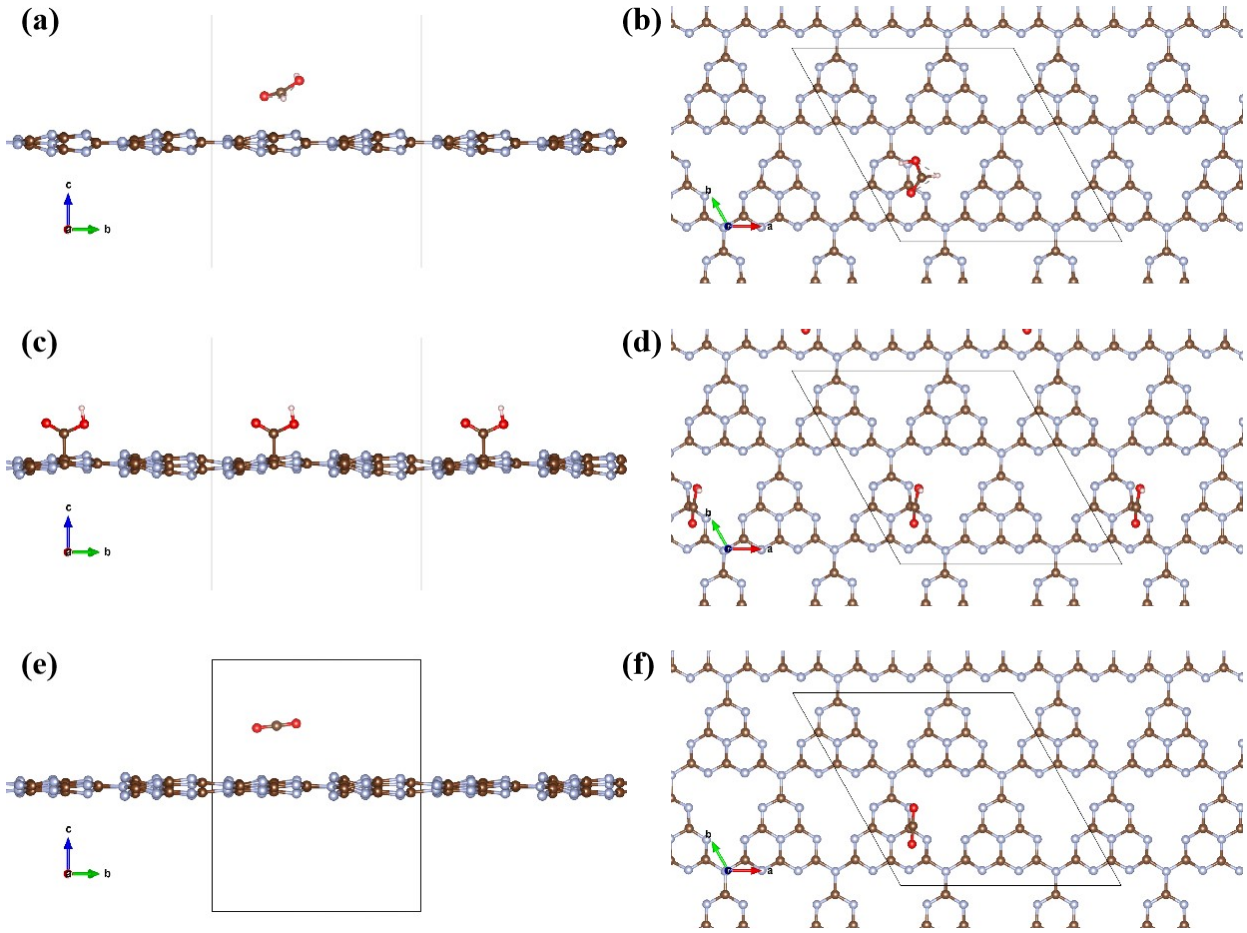

Fig. S13. Optimized Configurations for FA dehydrogenation pathways on g-C_3N_4. **(a)** Side view and **(b)** top view of the FA initial configuration on the g-C_3N_4. **(c)** Side view and **(d)** top view of the formate intermediate configuration on the g-C_3N_4. **(d)** Side view and **(e)** top view of CO_2 on the g-C_3N_4. (Red: O; white: H; brown: C; blue: N) by DFT calculation.

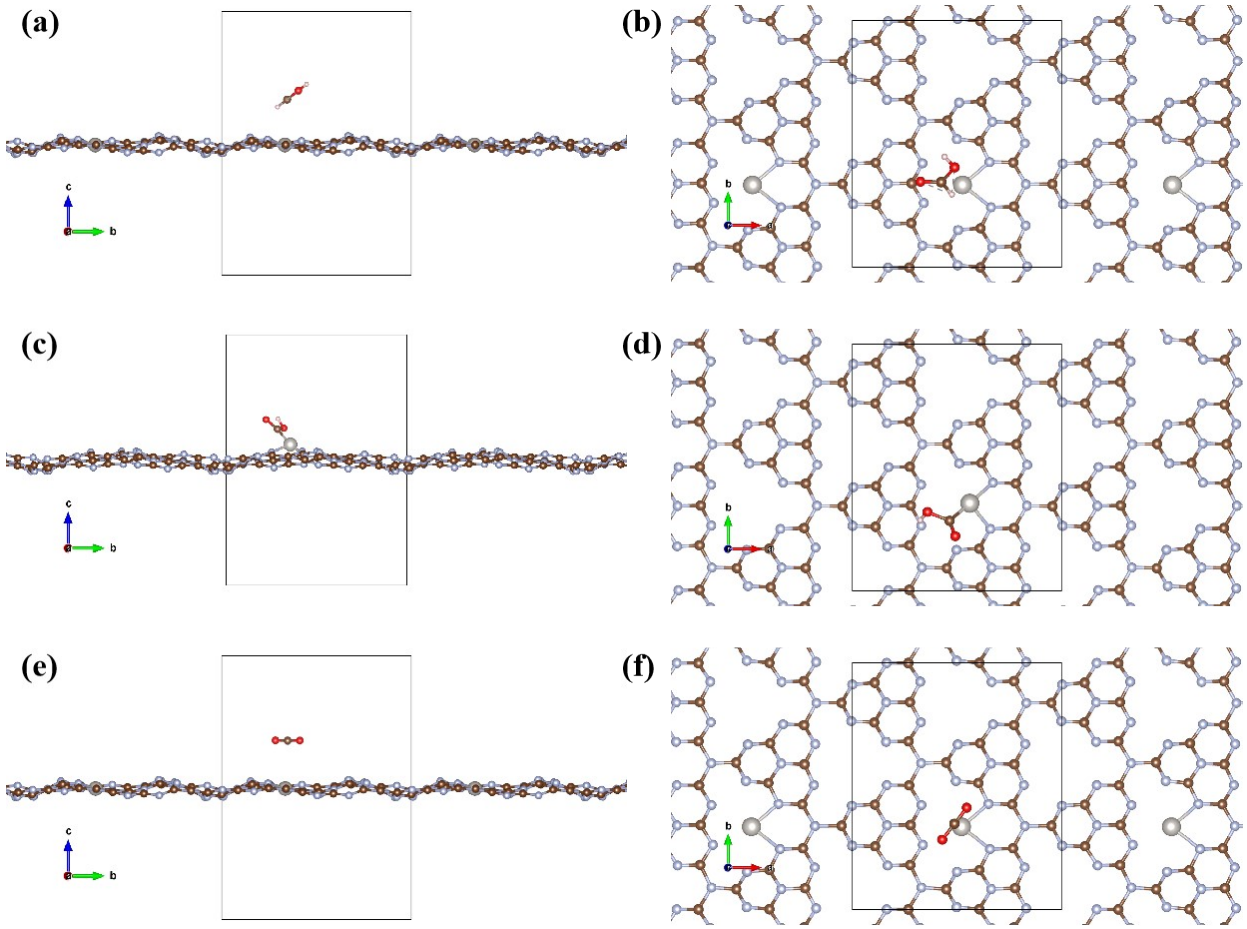

Fig. S14. Optimized Configurations for formic acid dehydrogenation pathways on 1.1 wt% Pt on g-C_3N_4. **(a)** Side view and **(b)** top view of the initial configuration of FA on 1.1 wt% Pt on g-C_3N_4. **(c)** Side view and **(d)** top view of the formate intermediate configuration on the 1.1 wt% Pt on g-C_3N_4. **(e)** Side view and **(f)** top view of CO_2 on the 1.1 wt% Pt on g-C_3N_4. (Red: O; white: H; brown: C; blue: N; grey: Pt) by DFT calculation.

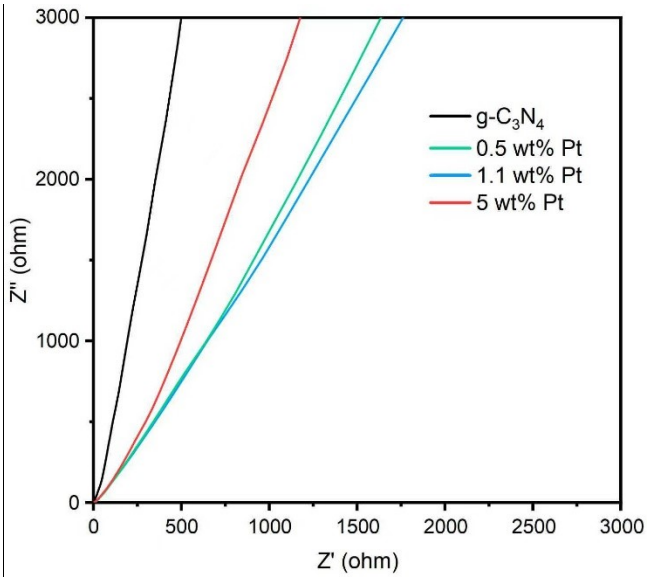

Fig. S15. EIS Nyquist plots of g-C_3N_4 and different Pt loading on g-C_3N_4.

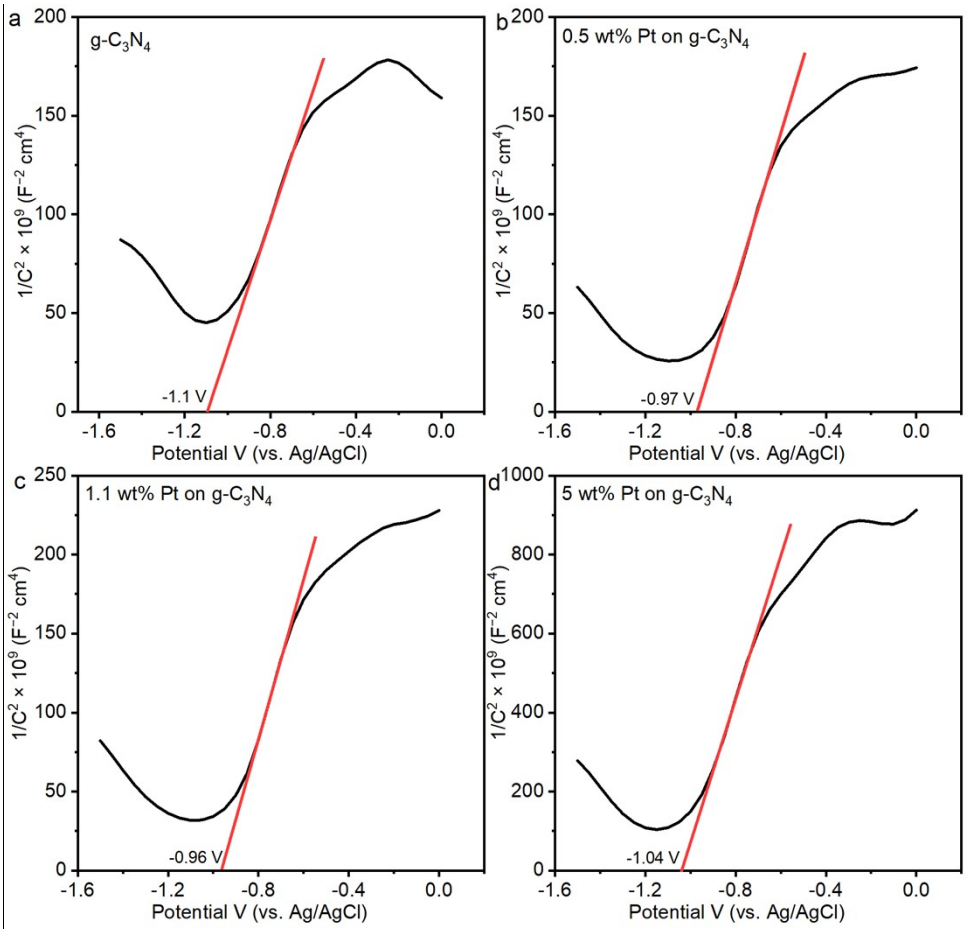

Fig. S16. Mott-Schottky plots of g-C_3N_4 and different Pt loading on g-C_3N_4.

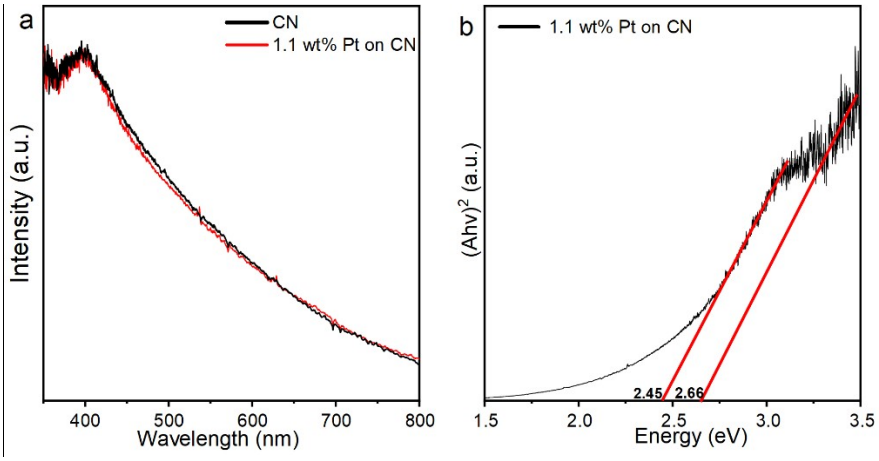

Fig. S17. (a) UV-vis spectrum of g-C_3N_4 and 1.1 wt% Pt on g-C_3N_4. **(b)** Tauc plots of 1.1 wt% Pt on g-C_3N_4. The apparent optical band gaps of 2.66 eV and 2.45 eV are obtained from linear fitting of different absorption edges. The higher value (2.66 eV) corresponds to the intrinsic band-to-band transition of g-C_3N_4, whereas the lower apparent gap (2.45 eV) is associated with Pt-induced localized electronic states near the band edge.

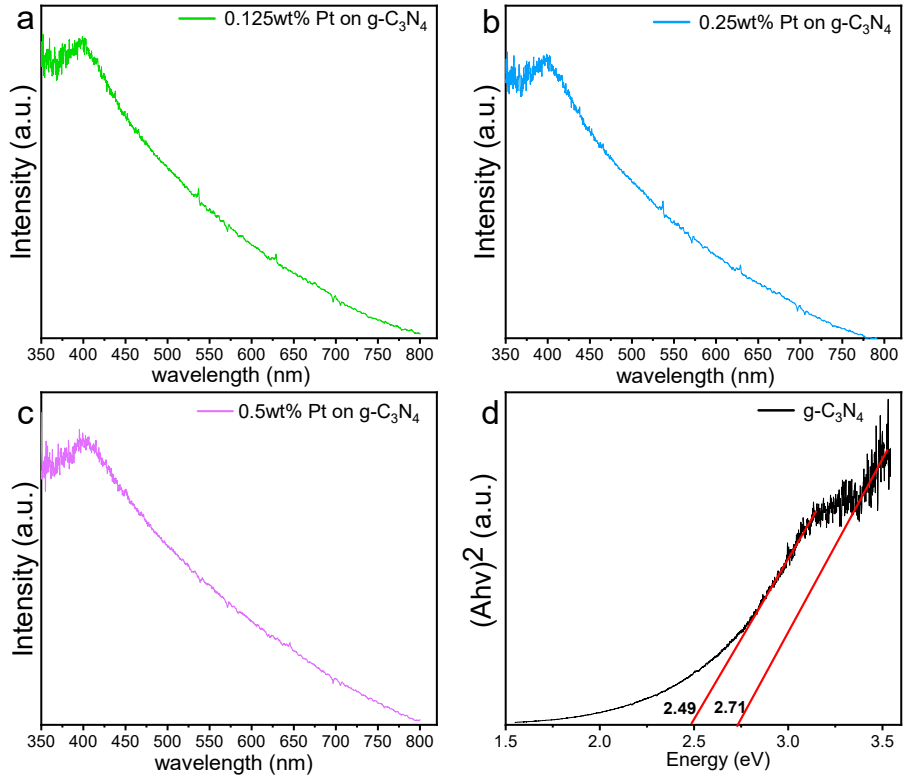

Fig. S18. UV-vis spectrum of **(a)** 0.125 wt% Pt on g-C_3N_4, **(b)** 0.25 wt% Pt on g-C_3N_4 and **(c)** 0.5 wt% Pt on g-C_3N_4 samples. **(d)** Tauc plots of pristine g-C_3N_4. For g-C_3N_4, the lower apparent optical gap (~2.49 eV) arises from intrinsic localized states and absorption tail near the band edge, which is a characteristic feature of polymeric g-C_3N_4, while the higher value (~2.71 eV) corresponds to the intrinsic band-to-band transition.

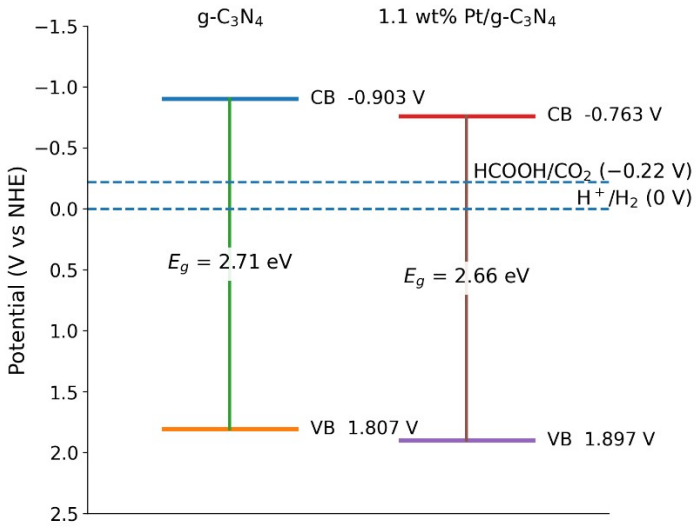

Fig. S19. Band alignment of g-C_3N_4 and 1.1 wt% Pt/g-C_3N_4 determined from Mott–Schottky analysis and UV-vis measurements.

References

1. Y. Li, L. Tang, S. Peng, Z. Li and G. Lu, *CrystEngComm*, 2012, **14**, 6974-6982.
2. H. Xu, H. Zhao, J. Xu, M. Eisapour, Z. Yu, H. Su, Y. Li, F. Zhou, J. Hu and Z. Chen, *ACS Applied Nano Materials*, 2024, **7**, 8804-8812.
3. Y. Li, R. He, P. Han, B. Hou, S. Peng and C. Ouyang, *Applied Catalysis B: Environmental*, 2020, **279**, 119379.
4. J. Sun, W. Zhen and C. Xue, *Applied Surface Science*, 2023, **623**, 157131.
5. X. Yuan, W. Zhen, S. Yu and C. Xue, *Chemistry–An Asian Journal*, 2021, **16**, 3683-3688.
6. H. Issa Hamoud, P. Damacet, D. Fan, N. Assaad, O. I. Lebedev, A. Krystianiak, A. Gouda, O. Heintz, M. Daturi and G. Maurin, *Journal of the American Chemical Society*, 2022, **144**, 16433-16446.
7. J. A. Nasir, M. Hafeez, M. Arshad, N. Z. Ali, I. F. Teixeira, I. McPherson and M. A. Khan, *ChemSusChem*, 2018, **11**, 2587-2592.
8. X. Ye, Y. Dong, Z. Zhang, W. Zeng, B. Zhu, T. Zhang, Z. Gao, A. Dai and X. Guan, *Frontiers in Energy*, 2024, 1-10.
9. Z. Zhang, S.-W. Cao, Y. Liao and C. Xue, *Applied Catalysis B: Environmental*, 2015, **162**, 204-209.
10. H. Liu, X. Liu, W. Yang, M. Shen, S. Geng, C. Yu, B. Shen and Y. Yu, *Journal of Materials Chemistry A*, 2019, **7**, 2022-2026.
11. L. Xiao, Y.-S. Jun, B. Wu, D. Liu, T. T. Chuong, J. Fan and G. D. Stucky, *Journal of Materials Chemistry A*, 2017, **5**, 6382-6387.
12. S. Zhang, M. Li, J. Zhao, H. Wang, X. Zhu, J. Han and X. Liu, *Applied Catalysis B: Environmental*, 2019, **252**, 24-32.
13. M. Wen, K. Mori, Y. Kuwahara and H. Yamashita, *ACS Energy Letters*, 2017, **2**, 1-7.
14. Z. Zhang, K. Liu, Y. Bao and B. Dong, *Applied Catalysis B: Environmental*, 2017, **203**, 599-606.
15. L.-L. Chu, *Catalysis Communications*, 2019, **128**, 105705.
16. S. Duan, S. Zhang, S. Chang, S. Meng, Y. Fan, X. Zheng and S. Chen, *International Journal of Hydrogen Energy*, 2019, **44**, 21803-21820.
17. M. Zhang, W. Lin, L. Ma, Y. Pi and T. Wang, *Chemical Communications*, 2022, **58**, 7140-7143.
18. Q. Li, J. Li, Y. Liu, J. Zhou, X. Yu, C. Hou, X. Liu, S. Cao and L. Piao, *Inorganic Chemistry*, 2024, **63**, 15034-15043.
19. R. M. Irfan, T. Wang, D. Jiang, Q. Yue, L. Zhang, H. Cao, Y. Pan and P. Du, *Angewandte Chemie International Edition*, 2020, **59**, 14818-14824.
20. T. Wang, M. Chen, J. Wu and P. Du, *Journal of Materials Chemistry A*, 2023, **11**, 2246-2251.
21. J. Wu, T. Wang, L. Zhang and P. Du, *ACS Sustainable Chemistry & Engineering*, 2024, **12**, 1625-1631.
22. T. Wang, L. Yang, D. Jiang, H. Cao, A. C. Minja and P. Du, *ACS Applied Materials & Interfaces*, 2021, **13**, 23751-23759.
23. S. Cao, Y. Chen, H. Wang, J. Chen, X. Shi, H. Li, P. Cheng, X. Liu, M. Liu and L. Piao, *Joule*, 2018, **2**, 549-557.
24. R. Muhammad Irfan, M. K. Zaman, M. H. Tahir, A. Ahmad, M. Tayyab, T. Ahmad, M. Hussain, I. Arshad and M. A. Shaheen, *ACS Applied Energy Materials*, 2023, **6**, 1834-1844.
25. H. Cao, T. Wang, A. C. Minja, D. Jiang and P. Du, *International Journal of Hydrogen Energy*, 2021, **46**, 32435-32444.

26. Y.-C. Chu, T.-J. Lin, Y.-R. Lin, W.-L. Chiu, B.-S. Nguyen and C. Hu, *Carbon*, 2020, **169**, 338-348.
27. K. Ding, A. Gulec, A. M. Johnson, N. M. Schweitzer, G. D. Stucky, L. D. Marks and P. C. Stair, *science*, 2015, **350**, 189-192.
28. J. Liu, M. Jiao, L. Lu, H. M. Barkholtz, Y. Li, Y. Wang, L. Jiang, Z. Wu, D.-j. Liu and L. Zhuang, *Nature communications*, 2017, **8**, 15938.
29. B. Zhang, H. Asakura, J. Zhang, J. Zhang, S. De and N. Yan, *Angewandte Chemie*, 2016, **128**, 8459-8463.
30. R. Kamai, K. Kamiya, K. Hashimoto and S. Nakanishi, *Angewandte Chemie*, 2016, **128**, 13378-13382.
31. L. Wang, R. Tang, A. Kheradmand, Y. Jiang, H. Wang, W. Yang, Z. Chen, X. Zhong, S. P. Ringer and X. Liao, *Applied Catalysis B: Environmental*, 2021, **284**, 119759.
32. X. He, Q. He, Y. Deng, M. Peng, H. Chen, Y. Zhang, S. Yao, M. Zhang, D. Xiao and D. Ma, *Nature communications*, 2019, **10**, 3663.
33. Z. Song, Y. N. Zhu, H. Liu, M. N. Banis, L. Zhang, J. Li, K. Doyle‐Davis, R. Li, T. K. Sham and L. Yang, *Small*, 2020, **16**, 2003096.
34. Y. Ren, Y. Tang, L. Zhang, X. Liu, L. Li, S. Miao, D. Sheng Su, A. Wang, J. Li and T. Zhang, *Nature communications*, 2019, **10**, 4500.
35. S. Liu, H. Xu, D. Liu, H. Yu, F. Zhang, P. Zhang, R. Zhang and W. Liu, *Journal of the American Chemical Society*, 2021, **143**, 15243-15249.
36. B. Qiao, A. Wang, X. Yang, L. F. Allard, Z. Jiang, Y. Cui, J. Liu, J. Li and T. Zhang, *Nature chemistry*, 2011, **3**, 634-641.
37. S. Yang, J. Kim, Y. J. Tak, A. Soon and H. Lee, *Angewandte Chemie International Edition*, 2016, **55**, 2058-2062.
38. H. Li, L. Wang, Y. Dai, Z. Pu, Z. Lao, Y. Chen, M. Wang, X. Zheng, J. Zhu and W. Zhang, *Nature nanotechnology*, 2018, **13**, 411-417.
39. X. Wu, H. Zhang, J. Dong, M. Qiu, J. Kong, Y. Zhang, Y. Li, G. Xu, J. Zhang and J. Ye, *Nano Energy*, 2018, **45**, 109-117.
40. X. Li, Z. Chen, Y. Yang, D. Huan, H. Su, K. Zhu, N. Shi, Z. Qi, X. Zheng and H. Pan, *Applied Catalysis B: Environmental*, 2022, **316**, 121627.
41. Y. Wu, Q. Wu, Q. Zhang, Z. Lou, K. Liu, Y. Ma, Z. Wang, Z. Zheng, H. Cheng and Y. Liu, *Energy & Environmental Science*, 2022, **15**, 1271-1281.
42. K. L. Zhou, Z. Wang, C. B. Han, X. Ke, C. Wang, Y. Jin, Q. Zhang, J. Liu, H. Wang and H. Yan, *Nature Communications*, 2021, **12**, 3783.
43. W. Tan, S. Xie, Y. Cai, H. Yu, K. Ye, M. Wang, W. Diao, L. Ma, S. N. Ehrlich and F. Gao, *Environmental Science & Technology*, 2023, **57**, 12501-12512.
44. L. Zhang, H. Liu, S. Liu, M. Norouzi Banis, Z. Song, J. Li, L. Yang, M. Markiewicz, Y. Zhao and R. Li, *ACS Catalysis*, 2019, **9**, 9350-9358.
45. Y. Feng, L. Dai, Z. Wang, Y. Peng, E. Duan, Y. Liu, L. Jing, X. Wang, A. Rastegarpanah and H. Dai, *Environmental Science & Technology*, 2022, **56**, 8722-8732.
46. J. Zhang, Y. Zhao, X. Guo, C. Chen, C.-L. Dong, R.-S. Liu, C.-P. Han, Y. Li, Y. Gogotsi and G. Wang, *Nature Catalysis*, 2018, **1**, 985-992.
47. J. Zhang, E. Wang, S. Cui, S. Yang, X. Zou and Y. Gong, *Nano Letters*, 2022, **22**, 1398-1405.
48. D. Kunwar, S. Zhou, A. DeLaRiva, E. J. Peterson, H. Xiong, X. I. Pereira-Hernández, S. C. Purdy, R. Ter Veen, H. H. Brongersma and J. T. Miller, *ACS catalysis*, 2019, **9**, 3978-3990.
49. S. Hejazi, S. Mohajernia, B. Osuagwu, G. Zoppellaro, P. Andryskova, O. Tomanec, S. Kment, R. Zbořil and P. Schmuki, *Advanced Materials*, 2020, **32**, 1908505.

50. J. Jones, H. Xiong, A. T. DeLaRiva, E. J. Peterson, H. Pham, S. R. Challa, G. Qi, S. Oh, M. H. Wiebenga and X. I. Pereira Hernández, *Science*, 2016, **353**, 150-154.
51. H. Xu, D. Lin, J. Shi, Z. Lv, X. Zhao, L. Ning, J. Xiao, L. Cui, J. Zhang and J. Yuan, *JACS Au*, 2024, **5**, 250-260.
52. H. N. Pham, A. DeLaRiva, E. J. Peterson, R. Alcala, K. Khivantsev, J. Szanyi, X. S. Li, D. Jiang, W. Huang and Y. Sun, *ACS Sustainable Chemistry & Engineering*, 2022, **10**, 7603-7612.
53. W. Zang, J. Lee, P. Tieu, X. Yan, G. W. Graham, I. C. Tran, P. Wang, P. Christopher and X. Pan, *Nature Communications*, 2024, **15**, 998.
54. Z. Xue, X. Gao, Y. Zhang, M. Yan, J. Xu and Y. Wu, *Chem Catalysis*, 2023, **3**.
55. Y. Kim, D. G. Oh, S. J. Cho, K. Khivantsev and J. H. Kwak, *Catalysis Today*, 2024, **425**, 114298.
56. K. Toukabri, S. Hejazi, M. Shahsanaei, S. Pour-Ali, A. Kosari, B. Butz, M. S. Killian and S. Mohajernia, *Langmuir*, 2024, **40**, 4661-4668.
57. S. Duan, R. Wang and J. Liu, *Nanotechnology*, 2018, **29**, 204002.
58. H. Li, Q. Wan, C. Du, Q. Liu, J. Qi, X. Ding, S. Wang, S. Wan, J. Lin and C. Tian, *Chem*, 2022, **8**, 731-748.